Characterization of the Changes in Secondary Structure and Architecture of Elastin−Mimetic Triblock Polypeptides during Thermal Gelation

Ajit Joseph M. D'Souza,[†,§] David S. Hart,[‡] C. Russell Middaugh,[§] and Stevin H. Gehrke*[,‡,§]

Molecular Biology, University of Wyoming, Laramie, Wyoming 82071, and Chemical and Petroleum Engineering and Pharmaceutical Chemistry, The University of Kansas, Lawrence, Kansas 66045

Received April 25, 2006; Revised Manuscript Received August 3, 2006

ABSTRACT: Vibrational spectroscopy and light scattering studies identify the conformational changes associated with gelation of elastin−mimetic triblock (EMT) copolymers. The EMT polypeptide is based on the VPGVG repeat of elastin and is constructed as a BAB triblock copolymer with relatively hydrophobic B-blocks. Laser Raman and ATR-FTIR spectroscopies probed changes in secondary structure associated with gelation in H_2O and D_2O. The amide I regions of these spectra suggest that the network-stabilizing interactions are intermolecular β-sheets with a significant fraction of the network containing β-turns and disordered structures. Peak frequency shifts in the ATR-FTIR spectra showed a conversion of extended hydrogen-bonded structures (polyproline II-like structures) to β-sheets during gelation. Molecular weights extrapolated through static light scattering at temperatures below the thermal transition were greater than for a single EMT chain. This suggests that some molecular organization exists prior to gelation, thus requiring relatively modest changes for molecular assembly to occur.

Introduction

The structural protein elastin found in the arterial walls, lungs, intestines, and skin of mammals imparts elasticity to these tissues. Native elastin is an insoluble, cross-linked protein that contains repeating sequences of VPGG, VPGVG, and APGVGV (V = valine, P = proline, G = glycine, A = alanine).[1] Studies of various elastin-like peptides containing the VPGVG sequence have shown that they are in a random coil conformation at low temperature, and as temperature rises they adopt a type II β-turn conformation.[2] On the basis of such studies, it was hypothesized that a series of type II β-turns (sterically allowed through the PG repeat) induces β-spiral formation, hypothesized as responsible for the elastic characteristics of the protein.[2,3] These polypeptides precipitate from aqueous solution upon heating above a temperature known as an inverse temperature transition (T_t) or a lower critical solution temperature (LCST). Substitutions at the second valine position can raise (if more hydrophilic) or lower (if more hydrophobic) this transition temperature without otherwise significantly changing the nature of the polypeptide. Because of the tunability of the material properties by modifying the sequence, biocompatibility, and facile production in recombinant *E. coli*, elastin-based materials have been the basis of considerable recent materials science, biomedical, and pharmaceutical research.[4−8]

Conticello and collaborators have developed a set of elastin−mimetic triblock (EMT) copolymers that self-assemble into elastic gels in aqueous solution upon heating.[9−14] The gelation is reversible upon cooling. The particular EMT studied here is a B−A−B block copolymer with a hydrophilic center block and hydrophobic end blocks. The hydrophobic end blocks, $[VPAVG(IPAVG)_4]_{16}$ (A = alanine, I = isoleucine), are believed to aggregate above the block's transition temperature to form a macroscopic gel.[11−14] The hydrophilic center block, $[(VPGVG)_2(VPGEG)(VPGVG)_2]_{30}$, contains the ionizable amino acid glutamic acid (E) which raises its thermal transition to a value higher than that of VPGVG when ionized. Although physical properties of this and similar polypeptides have been characterized,[9−11,13,14] the possible role of changes in secondary structure that may accompany gelation has not been investigated. We have shown that the properties of poly(α-L-lysine) gels are strongly dependent upon secondary structure.[15] Fully understanding the stabilizing interactions responsible for gelation and the factors affecting them is needed to tailor polypeptide materials for applications. For example, silk-elastin-like block polypeptides irreversibly gel,[4,7,8] while EMT gels are entirely reversible. Furthermore, while most physical gels either do not swell or dissolve when placed in excess solvent, EMT gel swells to a stable equilibrium without redissolution.[16] Above the gelation temperature, EMT gels are thermally responsive; that is, the swollen volume of the gels varies with temperature, much like poly(*N*-isopropylacrylamide) gel, which has been widely studied for applications as diverse as triggered drug delivery, biosensors, and separations.[17] Thus, it appears that EMT has stabilizing interactions strong enough to hold the gel together above the transition temperature, but with sufficient conformational flexibility to allow reversible swelling and shrinking in the gel state and yet not so stable as to form irreversible complexes as with silk−elastin block copolymers. In short, EMT is a thermally gelling and thermally responsive material—a very unusual combination of properties. Therefore, this study was undertaken to better understand the stabilizing interactions in this network, which should aid the design of polypeptide-based materials generally. Here we report on changes in the secondary structure and architecture of EMT during gelation.

Materials and Methods

Synthesis and Purification of EMT. Synthesis and purification of EMT were carried out following the basic procedure previously

[†] University of Wyoming.
[‡] Chemical and Petroleum Engineering, University of Kansas.
[§] Pharmaceutical Chemistry, University of Kansas.
* Corresponding author. E-mail: shgehrke@ku.edu.

10.1021/ma060915j CCC: $33.50
Published on Web 09/07/2006

reported by Wright and Conticello.[11,14] The *E. coli* strain BL21-Gold(DE3) containing the elastin−mimetic triblock plasmid was provided by Prof. Vincent P. Conticello of Emory University, and chemicals were acquired from Sigma-Aldrich (St. Louis, MO). Briefly, cultures of *E. coli* were grown for 36 h in Terrific Broth medium with kanamycin (50 μg/mL) at 37 °C and shaken orbitally in flasks at 175 rpm. Cells were subsequently harvested through centrifugation at 4000*g* at 4 °C for 20 min, and the pellets were resuspended in pH 8 lysis buffer (100 mM NaCl, 50 mM TRIS-HCl, 1 mM EDTA). Three freeze−thaw cycles were used to partially lyse the cells (−80 °C/25 °C). Upon partial lysis, lysozyme (1 mg/L of culture) and protease inhibitor cocktail (5 mL/L of culture) were added to the suspension and incubated for 30 min at 25 °C. Benzonase (0.175 IU/L of culture) and $MgCl_2$ (1 mM) were then added to the suspension and incubated at 4 °C for 12 h. The supernatant was recovered after centrifugation at 12000*g* for 45 min at 4 °C. A simple precipitation−redissolution process that takes advantage of the unusual solubility properties of elastin, known as thermal cycling, was used to purify EMT from other *E. coli* components. The precipitating cycle was performed by heating the supernatant (with NaCl added to 500 mM) to 37 °C followed by centrifugation at 18000*g* for 80 min. The supernatant was discarded, and the precipitate containing the EMT and other thermally precipitated materials was resuspended in lysis buffer at 4 °C. In the cold cycle at 4 °C, the EMT redissolves, and after centrifugation at 12000*g* for 80 min, pelleted solids are discarded. The thermal cycling is repeated several times until no solids precipitate even after shaking for 14−16 h at 4 °C. The final solution was dialyzed against water and lyophilized to yield dry, fibrous EMT protein.

FTIR Spectroscopy of EMT. Fourier transform infrared spectra were collected with an ABB Bomem Prota FT-IR spectrophotometer. A 10% w/w solution of EMT in deionized−ultrafiltered water was placed on a ZnSe ATR crystal, and spectra were collected from 2500 to 1000 cm^{-1}. Kinetic scans were collected as the sample warmed from 4 °C to room temperature over half an hour. The sample temperature was monitored using a thermocouple. To remove the contributions of H_2O in the amide I region, a blank H_2O spectrum was subtracted from the sample spectrum using Grams AI software. A flat baseline in the 2500−2000 cm^{-1} region was used as a measure of the extent of subtraction. Peaks in the 1600−1700 cm^{-1} range were assumed to be primarily due to the amide I band of EMT. The only side chain with a peak in this region was glutamic acid, whose total concentration was sufficiently low that it was not expected to contribute significantly to the total spectrum. This step was omitted from D_2O samples since this solvent does not have any vibrational bands in the 1600−1700 cm^{-1} region. A baseline correction was applied to yield a linear baseline with zero slope between 1800 and 1750 cm^{-1}. This baseline was assigned zero absorption units. The region of the spectrum between 1800 and 1500 cm^{-1} was then Fourier self-deconvolved employing a *K* factor of 2, followed by nine-point Savitsky−Golay smoothing. The resultant spectrum was then peak fitted by using a linear baseline, an initial full width at half-height (fwhh) of 13 cm^{-1}, and an optimum mixture of Gaussian and Lorentzian peak shapes. The peak positions were identified using a second-derivative spectrum of the Fourier self-deconvolved spectrum. Assuming identical extinction coefficients for each band in the amide I region, the relative contributions of the various secondary structure elements were calculated. This assumption is undermined by the work of de Jongh et al., who suggest that of all the secondary structures the sheets have the highest molar absorptivity,[18] whereas it is reinforced by the works of Chirgadze et al.[19] and Chirgadze and Brazhnikov,[20] who indicate that the extinction coefficient of the amide band is independent of the secondary structure. Considering the excellent correlation between secondary structure estimates and calculations from the atomic coordinates by Byler and Susi,[21] who assumed an equal extinction coefficient for all secondary structures, this assumption seems to be well-founded. Presently this assumption is commonly made when calculating the secondary structure fractions of proteins using FTIR, and thus we have followed this practice in this work.

Raman Spectroscopy of EMT. Raman spectra were recorded with a Chromex Raman 2000 equipped with a 300 mW 785 nm solid-state diode laser with backscattering geometry. Each Raman spectrum was collected at a discrete temperature after the sample had been held at thermal equilibrium for 20 min. As recommended by Williams,[22] the spectrum of water was subtracted from that of EMT such that the spectrum between 1730 and 1800 cm^{-1} was free of curvature and the linear extrapolation of this region intersected with the baseline at 1500−1520 cm^{-1}. The resultant spectra were peak fit as described above, but without using Fourier self-deconvolution.

Enzymatic Isolation of the End Blocks. For FTIR investigation of the B-blocks, EMT was digested with Endoproteinase GluC (New England Biolabs, Beverly, MA), a serine protease that cleaves peptide bonds on the C-terminal side of glutamic acid residues. A 20:1 molar ratio of EMT (4.5 mg) to GluC (50 μg) in GluC reaction buffer (7.5 mL of pH 8, 50 mM Tris buffer containing 0.5 mM diglutamic acid) (New England Biolabs, Beverly, MA) was shaken at 200 rpm for 16 h at room temperature (25 °C). Since the end blocks were insoluble in the reaction medium, they were isolated by centrifugation at 14000*g* for 30 min at 4 °C, and the supernatant containing the soluble center block fragments was discarded. The precipitate obtained was washed three times with deionized water to remove components of the buffer and the degraded hydrophilic center block.

FTIR Spectroscopy of the Elastin-like End Blocks. Precipitate from this solution (2 mg) was air-dried overnight in a hood at room temperature (25 °C), and the remaining film was crushed with KBr crystals (8 mg) and compressed into a pellet with a Carver press. The sample pellet was then analyzed with a Nicolet transmission cell (Thermo Nicolet, Madison, WI) on the same infrared spectrometer described above. Spectra of the B-blocks were collected from 2500 to 1000 cm^{-1} with 128 consecutive scans at a resolution of 4 cm^{-1} at 25 °C. Spectra were treated as described above, except no subtraction of contributions from water was implemented.

Static and Dynamic Light Scattering. Light scattering measurements were made using a dynamic light scattering (DLS) system (Brookhaven Instrument Corp., Holtsville, NY) consisting of a green diode 50 mW laser (532 nm), a BI-200SM multiangle goniometer, and a digital correlator (BI 9000AT). DLS measurements were obtained at an angle of 90° from the incident radiation and at an initial count of 100 kcps. For each light scattering measurement, an aqueous solution containing 0.1% w/w of EMT was prepared. Lyophilized EMT was dissolved in double distilled water at 4 °C; after 6 h, the solution was added to the scattering cell and given at least 30 min to equilibrate at the experimental temperature. At this low concentration, the protein does not significantly alter the viscosity of the solution or form a gel. For each sample, data were collected continuously for three 1 min intervals and averaged. From the autocorrelation function, the mean diffusion coefficient and the polydispersity index were determined by the method of cumulants using a quadratic fit. The effective hydrodynamic radius (R_h) was calculated from the diffusion coefficient by the Stokes−Einstein equation.

Static light scattering (SLS) measurements were made on EMT solutions prepared as they were for DLS measurements, but at concentrations ranging from 0.6 to 1.4 mg/mL of EMT. Measurements were made at 35, 45, 60, 75, 90, 105, and 120° using a 1 mm pinhole with intensities collected over ten 2 s periods. SLS data are analyzed using the Berry equation:[23]

$$\left(\frac{Kc}{R_\theta}\right)^{0.5} = \left(\frac{1}{M_w}\right)^{0.5}\left(1 + \frac{16\pi^2}{6\lambda^2}(R_g)^2 \sin^2\left(\frac{\theta}{2}\right) + ...\right)(1 + A_2 M_w c)$$

The optical constant, *K*, is defined as $K = (2\pi^2 n_0^2/\lambda^4 N_A)(dn/dc)^2$, where n_0 is the refractive index of the solvent, dn/dc is the differential refractive index, N_A is the Avogadro's number, θ is the scattering angle in degrees, λ is the wavelength, and c is the concentration of the particles. The dn/dc was measured using a differential refractometer (Optilab rEX, Wyatt Technology Corp., Santa Barbara, CA). Fitting the SLS data to the above equation

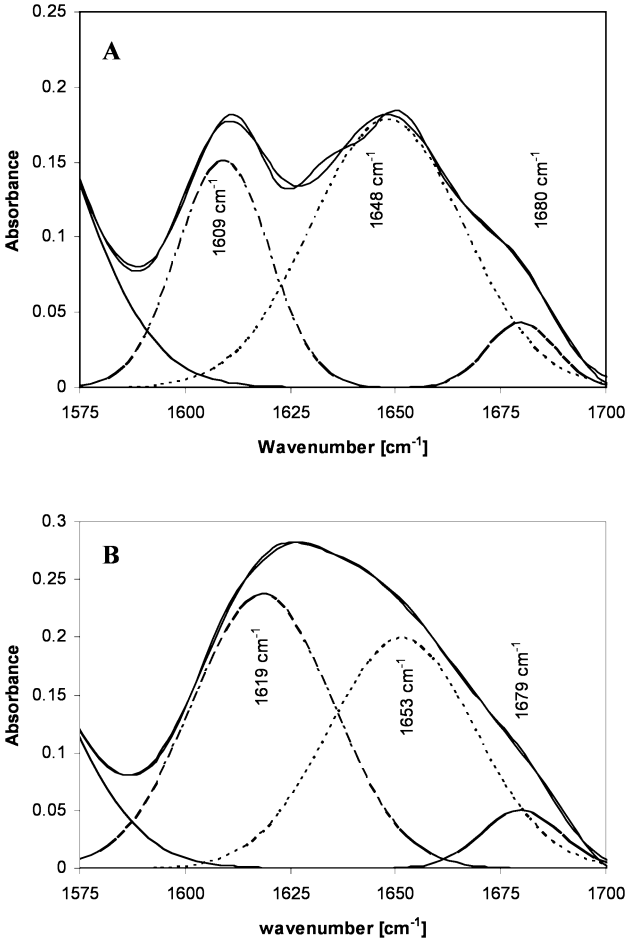

Figure 1. FTIR scans of EMT in water at 11 °C (A) and 21 °C (B). The phase transition occurs near 17 °C. The spectra were peak fit to yield the underlying bands. The band at 1609 cm^{-1} was assigned to extended PP-II helices, 1619 cm^{-1} to β-sheets, 1648 and 1653 cm^{-1} to unordered structures/α-helix, and 1679 and 1680 cm^{-1} to β-turns.

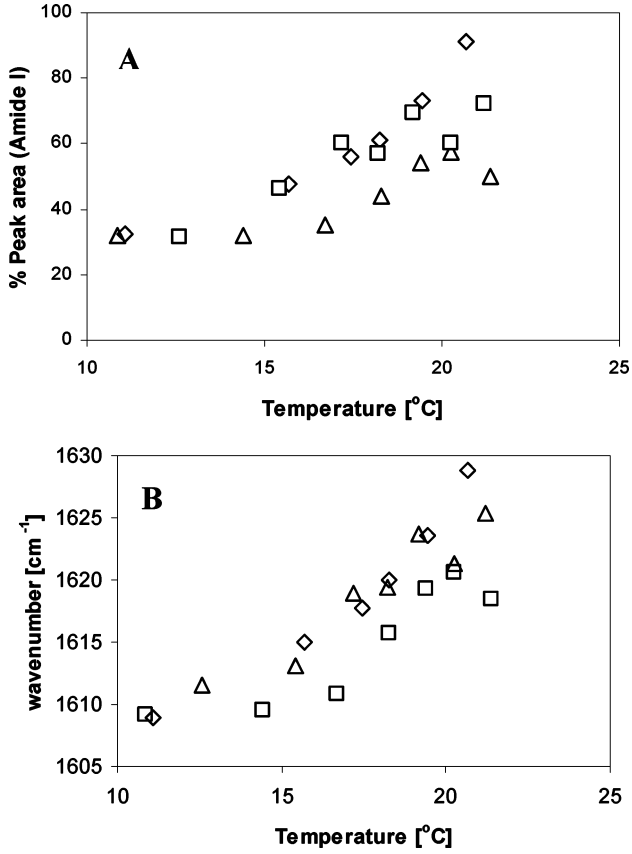

Figure 2. (A) Percent peak area of the frequency associated with PP-II-like structures and β-sheet in the ATR-FTIR spectrum of EMT in H_2O as a function of temperature. (B) Peak frequency shift of PP-II-like structures to β-sheet as a function of temperature. These figures show the result of three separate trials with symbols indicating separate trials.

yields a weight-averaged molecular weight (M_w), a radius of gyration (R_g), and the second virial coefficient (A_2).

Results

ATR-FTIR Spectra of EMT in H_2O. Representative ATR-FTIR spectra of EMT in water at temperatures above and below the gelation point (near 17 °C) are shown in Figure 1. The spectra are characterized by two broad asymmetric amide bands centered near 1609 and 1648 cm^{-1} below the gelation temperature and by a single asymmetric band centered at 1625 cm^{-1} above the gelation temperature. The shoulders and asymmetric nature of the bands suggest a composite of multiple peaks. Peak fitting of the ATR-FTIR spectra of EMT in water reveals three bands centered near 1610−1625, 1640−1655, and 1660−1680 cm^{-1}. During gelation, peaks shift from near 1610 cm^{-1}, which were assigned to hydrated, extended polyproline II-type helices (PP-II), to 1620−1625 cm^{-1}, which are attributed to intermolecular β-sheets. This peak shift was significant for three separate trials (Figure 2) and implies that PP-II-like structures convert to intermolecular β-sheets during gelation. A similar peak shift over this portion of the amide I region has been seen upon increases in temperature of 5 wt % aqueous solutions of poly(AVGVP) and poly(GVGVP).[24] Peaks in the range of 1640−1655 cm^{-1} were assigned to unordered structures/α-helices, and peaks in the range of 1660−1680 cm^{-1} were attributed to type II β-turns. The peak assignments above and below the gelation temperature (∼17 °C) are summarized in Table 1 with the average peak fit frequencies reported. It is apparent from Figure 2 that as the EMT gels, the fraction of β-sheet increases considerably while the peak associated with β-sheet red shifts 10−15 cm^{-1} from PP-II-like structures. The percent peak areas (in the amide I region) of both type II β-turn structures and unordered structures decreased on average 20% during gelation.

The assignments of bands due to β-sheets and unordered structures have been well documented[25] and do not require further elaboration here. The assignments of bands due to PP-II, however, may need further explanation. The PP-II structure is an extended helical structure originally proposed by Tiffany and Krimm.[26] This conformation is devoid of internal hydrogen bonding, and therefore these secondary structure elements cannot be identified by intramolecular hydrogen-bonding patterns, as is regularly done for other types of secondary structure. The length of PP-II segments is expected to be shorter (4−8 residues) than α-helical or β-sheet units. This follows from the lack of stabilizing intramolecular hydrogen bonds.[27] For the same reason, PP-II helices are more flexible than α-helices. PP-II helices have a rise per residue almost twice as of α-helices and thus are much longer on a per residue basis. The main chain of PP-II is also more solvent accessible.[28] PP-II helices appear to be stabilized by a regular pattern of main chain−water hydrogen bonds.[29] The formation of these strong hydrogen bonds would be expected to produce a correspondingly lower frequency amide I band. Therefore, the band at 1612 cm^{-1} has been attributed to PP-II.[25] Similar bands have also been observed in β-lactoglobulin by Lefèvre and Subirade.[30]

Table 1. Summary of ATR-FTIR and Raman Peak Assignments in the Amide I Region[a]

	ATR-FTIR in H_2O		ATR-FTIR in D_2O	
	frequency [cm^{-1}]	conformation	frequency [cm^{-1}]	conformation
below 17 °C	1611	PP-II helices	1621	β-sheet
	1643	unordered	1643	unordered
	1670	type II β-turn	1665	type II β-turn
above 17 °C	1621	β-sheet	1624	β-sheet
	1647	unordered	1645	unordered
	1674	type II β-turn	1665	type II β-turn

Raman in H_2O		Raman in D_2O	
Raman shift [cm^{-1}]	conformation	Raman shift [cm^{-1}]	conformation
1610−1611	PP-II helices	1608−1610	PP-II helices
1627−1629	β-sheet	1622−1631	β-sheet
1645−1647	unordered	1644−1656	unordered
1665−1668	type II β-turns	1662−1669	type II β-turns
1683−1684	high-frequency β-sheet	1682−1684	high-frequency β-sheet

[a] ATR-FTIR average peak frequencies are reported above and below the gelation temperature of 17 °C. Raman bands attributed to each conformation showed a maximum within the range listed in the frequency column. In the text and figures, the average band frequency has been cited in lieu of the range listed here.

FTIR Spectra of EMT in D_2O. The spectra of EMT in D_2O are characterized by two broad asymmetric amide bands centered at 1620 and 1640 cm^{-1} below the gelation temperature and by a single asymmetric band centered at 1630 cm^{-1} above the gelation temperature. Peak fitting of all spectra reveals three separate bands centered near 1621, 1643, and 1665 cm^{-1}. As above, the band at 1621 cm^{-1} is attributed to a mixture of hydrated, extended polyproline II helices (PP-II) and intermolecular β-sheets. The peak at 1621 cm^{-1} did red shift after gelation (3 cm^{-1}); however, the shift was not as significant as seen in H_2O. The band at 1640 cm^{-1} is consistent with the presence of unordered structures, especially when the band is compared with that observed in H_2O at 1643−1648 cm^{-1}. The deuteration of the amide protons in unordered structures is known to induce band shifts to lower frequencies of this magnitude.[31] Although the presence of 3_{10} helices[25,32] or type III β-turns[33,34] has been shown to produce a band at 1640 cm^{-1}, it seems less likely that these structures exist in EMT to contribute to this band. The band at 1665 cm^{-1} is assigned to type II β-turns.[35]

In the presence of D_2O, the spectral bands representative of each type of secondary structure are not as clearly resolved as in the presence of H_2O; some of the fit peaks appear to represent composites of signals due to at least two different types of secondary structures. Despite this, the spectra do demonstrate some clear trends in terms of structural changes. As the protein gels, the fraction of β-sheet increased slightly while the peak near 1621 cm^{-1} shifted away from PP-II-like structures to β-sheet. The contributions from the disordered portion of the protein and type II β-turns appear to be relatively unaffected by the sol−gel transition.

Raman Spectra of EMT in H_2O. The Raman spectra of EMT in the sol and gel states are shown in Figure 4. The amide I region of the Raman spectra of EMT was characterized by two maxima at 1676 and 1613 cm^{-1}. Peak fitting resolved five major components centered near 1684, 1667, 1646, 1628, and 1610 cm^{-1}. The peak at 1646 cm^{-1} can be assigned to α-helices plus unordered structures[36,37] and the peak at 1610 cm^{-1} to PP-II-type extended hydrogen-bonded structures. A Raman band at 1610 cm^{-1} is typically attributed to the presence of tyrosine rather than the amide bonds. It has, however, been observed in proline-containing peptides[38] that lack tyrosine (as EMT does). Peaks at 1628 and 1684 cm^{-1} are known to represent the lower and higher frequency shifts of β-sheets. The band at 1667 cm^{-1} has also been shown to be characteristic of β-sheets,[36,37,39] but Thomas et al.[40] have argued that the band due to the type II β-turn of poly(VPGVG) (MW ∼ 100 kDa) also appears at the same frequency. Since the VPGVG repeat has also been shown through 2D NMR to form type II β-turns in aqueous solution,[41] this band was assigned to type II β-turns. These secondary structure conformations are consistent with the conclusions drawn from the FTIR spectra of EMT in H_2O.

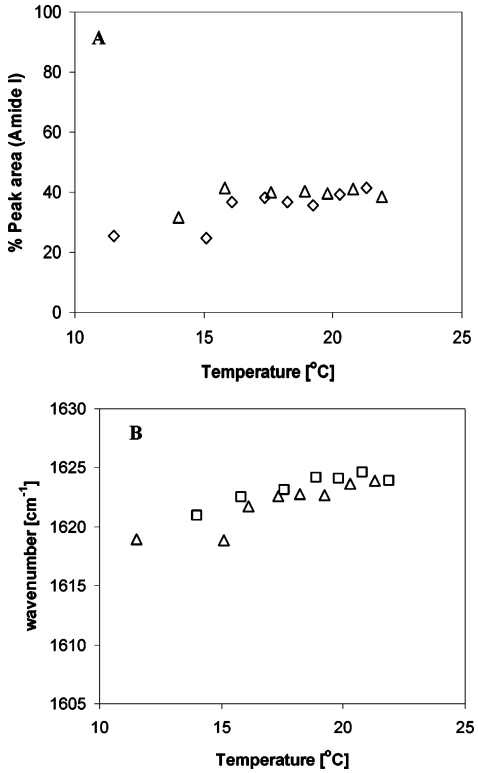

Figure 3. (A) Percent peak area of the frequency associated with PP-II-like structures and β-sheet in the ATR-FTIR spectrum of EMT in D_2O as a function of temperature. (B) Peak frequency shift of PP-II-like structures to β-sheet as a function of temperature. These figures show the result of two separate trials with symbols indicating separate trials.

From Figure 5 it is evident that as EMT passes from sol to gel, the area associated with the β-sheet band increases, whereas that associated with extended PP-II-like structures decreases. This observation is also consistent with the with FTIR results.

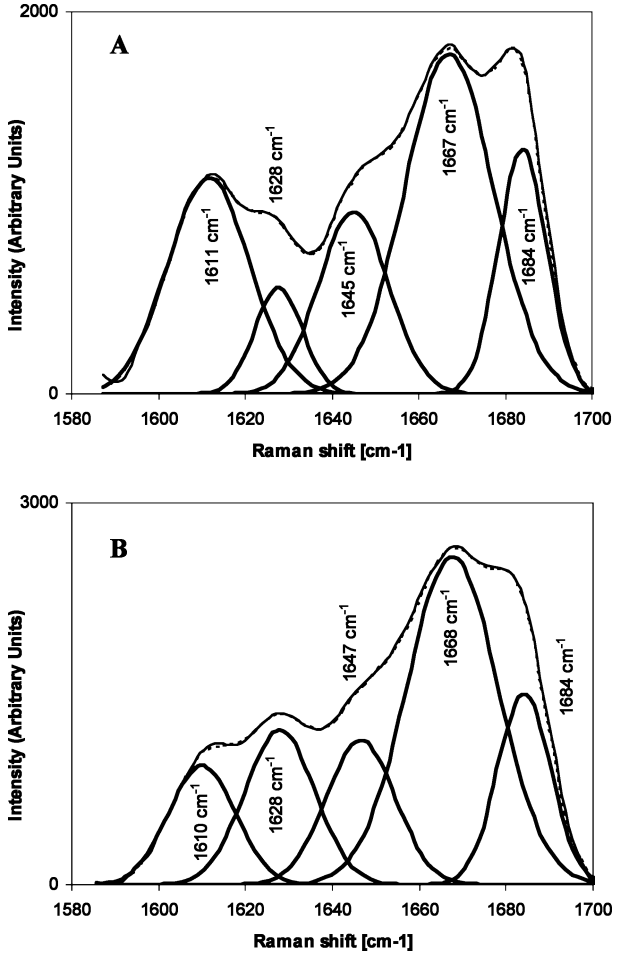

Figure 4. Raman scans of EMT in water at 10 °C (A) and 22.5 °C (B). The phase transition occurs near 17 °C. The spectra were peak fit to yield the underlying bands. The band at 1610−1611 cm^{-1} was assigned to extended PP-II helices, 1628 and 1684 cm^{-1} to β-sheets, 1645−1647 cm^{-1} to unordered structures, and 1667−1668 cm^{-1} to a combination of β-sheets and β-turns.

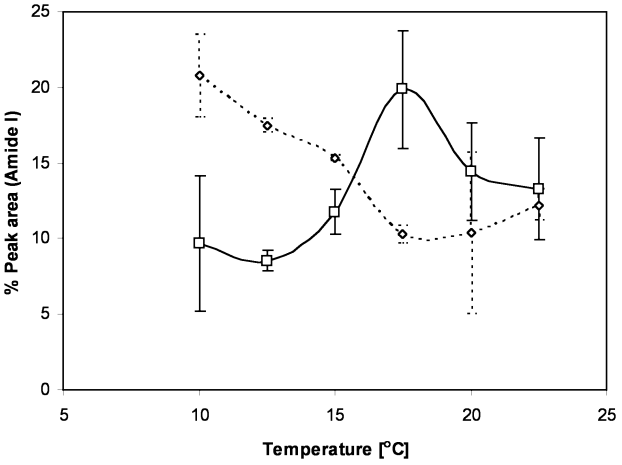

Figure 5. Raman spectrum of EMT in H_2O changes as a function of temperature. This figure shows the changes in the various underlying bands that contribute to the spectra: β-sheets (1628 cm^{-1}) [open squares] and PP-II (1610 cm^{-1}) [open diamonds]. As the temperature increases, the PP-II helices decrease and the β-sheets increase.

Raman Spectra of EMT in D_2O. The amide I region of the Raman spectra of EMT in D_2O were characterized by two maxima at 1671 and 1610 cm^{-1}. Peak fitting revealed five components centered near 1684, 1666, 1649, 1627, and 1609 cm^{-1}, consistent with the fits obtained from spectra of EMT in water.

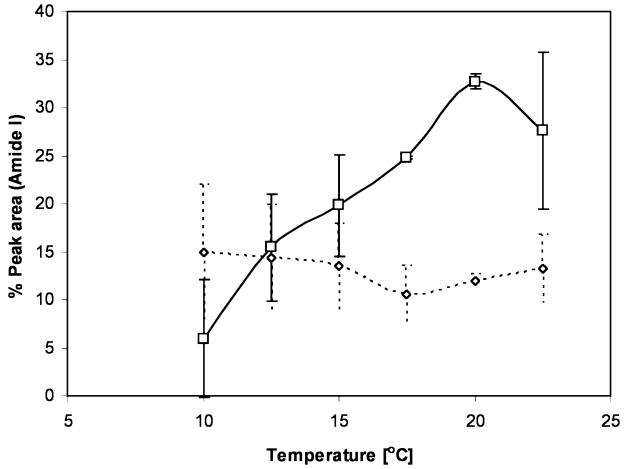

Figure 6. Raman spectrum of EMT in D_2O changes as a function of temperature. This figure shows the changes in the various underlying bands that contribute to the spectra: β-sheets (1627 cm^{-1}) [open squares] and PP-II (1609 cm^{-1}) [open diamonds]. As the temperature increases, the PP-II helices decrease and the β-sheets increase.

These peaks were assigned to the same conformations deduced to be present in the water spectra. The change in the secondary structure of EMT during gelation in D_2O is similar to that seen in H_2O. Figure 6 shows the changes in secondary structure content with temperature. It is apparent that the PP-II structures decrease slightly whereas the β-sheets significantly increase. Although in D_2O the changes in secondary structure of EMT during gelation are not as pronounced as in H_2O, the trends observed are similar to those observed in H_2O (Figure 6).

FTIR Spectrum of the End Block Precipitate. It is presumed on the basis of the structural integrity of the EMT gel that the type II β-turns are localized to the A blocks and β-sheet structures to the B blocks. As previously mentioned, the VPGVG repeat is known to form a type II β-turn, and this repeat only exists in the A block. The presence of the type II β-turns in the A blocks provides a potential explanation for the thermally responsive behavior (i.e., reversible swelling and shrinking) of EMT in the gel state as occurring through an intramolecular conformational change. Therefore, to better resolve the local conformation of the blocks and assign secondary structures to specific regions, EMT was digested with GluC. This enzymatic digest did not precisely cut between the A and B blocks because the A-block sequence is VPGVG[$(VPGVG)_2$-VPGEG$(VPGVG)_2]_{30}$VPGVG. At most, however, 18 amino acids containing the VPGVG sequence could remain attached to the B block after digestion. Therefore, it was assumed that the absorbance due to the higher concentration of B-block amino acids (410 amino acids/per B block) would greatly outweigh this small percentage (5%) of β-turn structure. Additionally, it was assumed by recovering the precipitated B blocks at 4 °C with centrifugation that all digested, fragmented portions of the A block remained in the supernatant because the transition temperature of the A block is greater than 25 °C at 5 wt %.[42] A total of eight peaks were fit to the B-block spectrum, with two additional peaks (fit outside of the amide I region) necessary to accurately simulate the sum of the peak fits with the recorded spectrum. The FTIR spectrum of the elastin-like end blocks of EMT in the solid state is shown in Figure 7. This spectrum is dominated by the presence of bands representative of β-turns and β-sheet. The high β-sheet content suggests that the intermolecular attractive interactions resulting from association of the end blocks are responsible for gel formation. The high β-turn content is consistent with the lack of PP-II-type structure

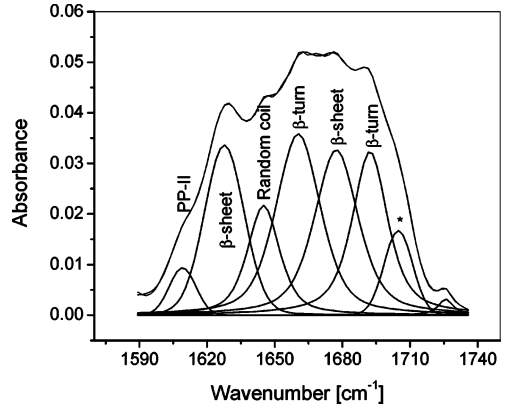

Figure 7. The dominant presence of β-sheet (19.8% at 1677 cm^{-1} and 23.5% at 1627 cm^{-1}) and β-turn (16.3% at 1693 cm^{-1} and 20.7% at 1661 cm^{-1}) conformations in the end-block aggregates suggests that these end blocks are involved in intermolecular contacts. This figure shows the FTIR spectrum of the end blocks. The band at 1706 cm^{-1} (indicated by asterisk) is due to C═O stretching of the COOH group of residual diglutamic acid.

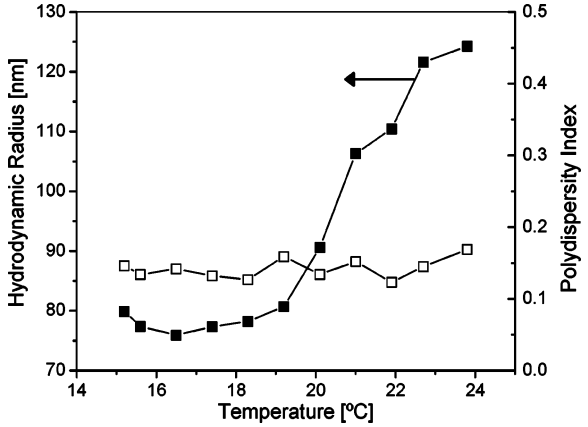

Figure 8. Hydrodynamic radius (R_h) increases with temperature, indicating an increase in aggregation number. This figure shows the R_h [solid squares, left axis] and polydispersity [open squares, right axis] of a 1 mg/mL solution of EMT as a function of temperature.

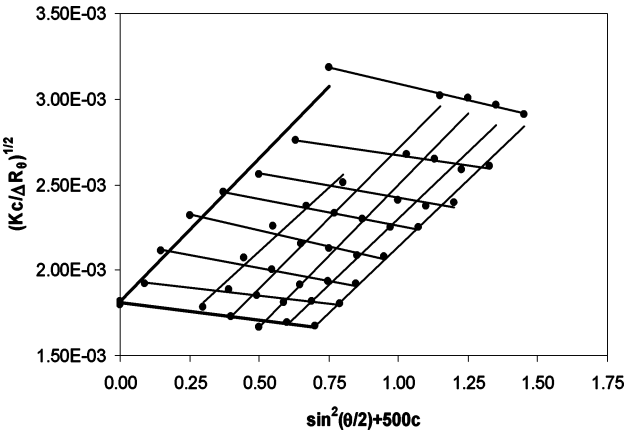

Figure 9. Representative Berry plot at 15 °C. Static light scattering experiments indicate that the radius of gyration (R_g) of EMT increases from 77 nm at 15.5 °C to 83 nm at 23.8 °C while the molecular weight increases from 310.31 to 484.79 kDa. The second virial coefficients were -2.0×10^{-4} at 15 °C and -4.6×10^{-4} cm^3 mol/g^2 at 24 °C.

that has been lost in favor of the β-turn due to the absence of water in this experiment.

Thus far, our observations indicate that β-sheets are an integral component of EMT structure in addition to the well-established role of β-turns.[43,44] The spectral frequency associated with this β-structure strongly suggests the presence of intermolecular β-sheets. It is also apparent that the extent of change in the secondary structure of EMT upon transition from the sol to the gel state is modest; this might at first seem counterintuitive when considered in the context of the dramatic macroscopic changes in physical properties that accompany this transition. Therefore, it was hypothesized that the organization that results in gel formation is preceded by molecular events at an intermediate level between monomeric species and the gelled network. To detect any such pregel organization, light scattering studies were undertaken.

Dynamic and Static Light Scattering. EMT forms a gel at a modest temperatures (∼17 °C) when dissolved in water at a sufficiently high concentration (>2.5 wt %). Gelation results from the formation of a network of intermolecular contacts. DLS studies were undertaken to better understand the rise in the intermolecular interactions with temperature. The concentration of EMT was held at 1 mg/mL, low enough to avoid gelation. This permits observation of any change prior to actual gelation. Figure 8 shows the dependence on mean particle size and polydispersity index of EMT on temperature. The effective R_h of the EMT molecule at 15 °C was observed to be ∼75 nm, significantly larger than the ∼7 nm observed for a typical globular protein of a similar molecular weight. With an increase in temperature, the R_h was observed to increase to ∼125 nm. These observations suggest that the entities that scatter the light are very large and imply that the scattering is primarily from multimers of EMT or that small amounts of contaminating high molecular weight material is distorting the estimate of mean particle size (the latter possibility reflects the much greater scattering by the larger particles). A polydispersity index of 0.15−0.2 was observed. Polydispersity in this context is a measure of the relative variance of the hypothetical Gaussian distribution centered on the R_h. Low polydispersity indicates a narrow distribution whereas a high polydispersity indicates a broader distribution or multiple families of particles. Monodisperse globular proteins may manifest polydispersities as low as 0.02. Thus, in this case, the high polydispersity index also suggests the presence of a distribution of aggregates at all temperatures. This is consistent with the observation of intermolecular β-sheets in the sol state using vibrational spectroscopy. These aggregates increase in size with increasing temperature, consistent with the increase in β-sheet content observed upon gelation.

To further characterize these associating species, static light scattering measurements were performed over a concentration range of 0.6−1.4 mg/mL. Since a conventional Zimm plot showed an upward curvature typical of branched polymers, the data were linearized using a Berry plot. A representative Berry plot is shown in Figure 9. From these plots and using an experimentally determined dn/dc of 0.2234 mL/g, the molecular weight of the scattering species was calculated to be 310 kDa at 15.5 °C and 485 kDa at 23.8 °C, confirming the presence of associated species not only at temperatures above the trasition temperature but also below it. Furthermore, the negative second virial coefficients (-2.0×10^{-4} at 15 °C and -4.6×10^{-4} cm^3 mol/g^2 at 24 °C) suggest an unfavorable interaction of EMT with water, also implying that EMT molecules have a greater affinity for each other than the aqueous medium. This affinity of EMT with itself increases with increasing temperature. Static light scattering experiments also indicate that the R_g of EMT increases from 77 nm at 15.5 °C to 83 nm at 23.8 °C. The ratio $\rho = R_g/R_h$ is a structure-sensitive parameter that is indicative of the deviation of the particle shape from sphericity. A sphere is characterized by a ρ parameter of 0.77.[45] The ρ parameter for EMT was found to be 1.0 at 15.5 °C and 0.66 at 23.8 °C,

suggesting that at lower temperature the aggregates may be somewhat elongated or star-shaped but approach a microgel-like shape, typically characterized by a dense core with dangling chains on the surface, at higher temperatures.[45−47] This is consistent with the micelle-like association of the end blocks as proposed by Wright and Conticello.[11]

Discussion

The ATR-FTIR and Raman spectra of EMT show significant amounts of β-sheet above and below the gelation temperature. Gelation of EMT, however, is accompanied by an increase in the β-sheet content. A decrease in the hydrated PP-II-type structures with temperature suggests that dehydration of these regions of the protein in favor of intermolecular β-sheet formation, as seen in Raman spectra of EMT in water. ATR-FTIR spectra similarly show a significant peak shift from PP-II-type structures to β-sheet in water. This shift was also seen in D_2O, but to a lesser extent. In comparing the ATR-FTIR spectra of EMT in water and D_2O, the extent to which β-sheet increases on a percent peak area basis during gelation is apparently related to the size of the peak shift from PP-II-type structures in the sol state. The β-sheet content increased to a greater extent in water over D_2O. This agrees with the well-established stabilizing effect of D_2O.[48] These two types of vibrational spectroscopies also show that gelation is accompanied by a modest decrease in unordered structure and β-turns. Interestingly, end block sequences in the solid state showed a secondary structure dominated by β-sheet and β-turns. This strongly suggests that the end blocks are involved in the intermolecular contacts and that they have a propensity to form β-turns as has been previously hypothesized.[49] Overall, however, it seems that in its hydrated form EMT does not prefer the β-turn conformation as previously observed with other peptides.[50] This deviation, however, needs to be evaluated in light of the concentrations studied. The studies reported heretofore on peptides have been conducted at low concentrations of about 0.1 mg/mL, whereas this study was conducted at a concentration of 100 mg/mL, more than a 1000-fold higher. Under these experimental conditions, EMT exhibits substantial intermolecular β-sheets above and below the gelation temperature, suggesting that intermolecular contacts exist in the EMT solution in the sol state, prior to gelation. In particular, the light scattering data are consistent with the presence of intermolecular contacts below the transition temperature. The changes in the R_h in the region of the gelation temperature but at a concentration where macroscopic gelation does not occur strongly suggest the formation of larger aggregates, apparently due to the formation of intermolecular β-sheet. The change in the second virial coefficient with temperature is also consistent with the dehydration of the PP-II-type structures to form β-sheets. The change in R_g suggests that as the aggregates become larger, they approach sphericity. This is consistent with the model proposed by Wright et al. for the gelation of EMT.[12] Assuming that only the end blocks are involved in gelation, it can be proposed that in the solid state the end blocks exhibit secondary structures dominated by β-turns. Upon hydration below the lower critical solution temperature, however, significant portions of the end blocks convert to extended, hydrated structures characterized by a PP-II-type conformation. Recently, Schmidt et al.[24,51] and Kurkova et al.[52] have proposed the presence of similar extended polymer chains below the critical solution temperature in elastin-like polypeptides, poly(GVGVP) and poly(AVGVP). The presence of β-sheets, also observed by Schmidt et al.,[24] along with the aggregates revealed by the light scattering data below the transition temperature suggests that a precursor of gelation-competent species (i.e., a stable pregelation intermediate) is present even in the sol state. As the temperature is raised, the PP-II-type structures engage in intermolecular β-sheet formation and gelation occurs. The well-established tendency of apolar interactions to increase in strength with temperature and the dominant stabilization of β-structures by such interactions between side chains is probably a driving force for this phenomenon.

Conclusions

Vibrational spectroscopy studies of the gelation of EMT demonstrate that gel formation is accompanied by significant changes in the secondary structure of this elastin-like polypeptide. However, an abrupt change in secondary structure is not required to form a gel. Similarly, light scattering studies argue that the phenomenon of EMT gelation is much more complex than a model of the conversion of isolated molecules aggregating to form a macroscopic complex at the sol−gel transition. Taken as a whole, these experiments strongly suggest that some level of organization exists prior to gelation and that macroscopic gelation results from relatively modest, but important, structural changes at the molecular level.

Acknowledgment. This work was supported by KBRIN (Kansas Biomedical Research Infrastructure Network) Grant NIH 5P20 RR164575-02, NIH NIGMS (National Institute of General Medical Sciences) Grant GM08359, and NSF Grant MCB0236039. We thank Prof. Vincent P. Conticello of Emory University for the cultures containing the EMT plasmid and helpful advice.

References and Notes

(1) Foster, J. A.; Bruenger, E.; Gray, W. R.; Sandberg, L. B. *J. Biol. Chem.* **1973**, *248*, 2876−9.
(2) Urry, D. W.; Shaw, R. G.; Prasad, K. U. *Biochem. Biophys. Res. Commun.* **1985**, *130*, 50−7.
(3) Urry, D. W.; Parker, T. M. *J. Muscle Res. Cell Motil.* **2002**, *23*, 543−59.
(4) Haider, M.; Megeed, Z.; Ghandehari, H. *J. Controlled Release* **2004**, *95*, 1−26.
(5) Chilkoti, A.; Dreher, M. R.; Meyer, D. E. *Adv. Drug Delivery Rev.* **2002**, *54*, 1093−111.
(6) Kopecek, J. *Eur. J. Pharm. Sci.* **2003**, *20*, 1−16.
(7) Megeed, Z.; Cappello, J.; Ghandehari, H. *Adv. Drug Delivery Rev.* **2002**, *54*, 1075−91.
(8) Megeed, Z.; Haider, M.; Li, D.; O'Malley, B. W., Jr.; Cappello, J.; Ghandehari, H. *J. Controlled Release* **2004**, *94*, 433−45.
(9) Nagapudi, K.; Brinkman, W. T.; Leisen, J.; Thomas, B. S.; Wright, E. R.; Haller, C.; Wu, X.; Apkarian, R. P.; Conticello, V. P.; Chaikof, E. L. *Macromolecules* **2005**, *38*, 345−54.
(10) Nagapudi, K.; Brinkman, W. T.; Thomas, B. S.; Park, J. O.; Srinivasarao, M.; Wright, E.; Conticello, V. P.; Chaikof, E. L. *Biomaterials* **2005**, *26*, 4695−706.
(11) Wright, E. R.; Conticello, V. P. *Adv. Drug Delivery Rev.* **2002**, *54*, 1057−73.
(12) Wright, E. R.; Conticello, V. P.; Apkarian, R. P. *Microsc. Microanal.* **2003**, *9*, 171−82.
(13) Wright, E. R.; McMillan, R. A.; Cooper, A.; Apkarian, R. P.; Conticello, V. P. *Polym. Prepr. (Am. Chem. Soc., Div. Polym. Chem.)* **2001**, *42* (2), 90−1.
(14) Wright, E. R.; McMillan, R. A.; Cooper, A.; Apkarian, R. P.; Conticello, V. P. *Adv. Funct. Mater.* **2002**, *12*, 149−54.
(15) Oliveira, E. D.; Hirsch, S. G.; Spontak, R. J.; Gehrke, S. H. *Macromolecules* **2003**, *36*, 6189−201.
(16) Hart, D. S.; Hagan, S. A.; Gehrke, S. H.; Conticello, V. P. *Controlled Release Soc. Trans.* **2004**, *31*, 133.
(17) Gehrke, S. H. *Adv. Polym. Sci.* **1993**, *110*, 81−144.
(18) de Jongh, H. H.; Goormaghtigh, E.; Ruysschaert, J. M. *Anal. Biochem* **1996**, *242*, 95−103.
(19) Chirgadze, Y. N.; Shestopalov, B. V.; Venyaminov, S. Y. *Biopolymers* **1973**, *12*, 1337−51.
(20) Chirgadze, Y. N.; Brazhnikov, E. V. *Biopolymers* **1974**, *13*, 1701−12.

(21) Byler, D. M.; Susi, H. *Biopolymers* **1986**, *25*, 469−87.
(22) Williams, R. W. *Methods Enzymol.* **1986**, *130*, 311−31.
(23) Tanner, D. W.; Berry, G. C. *J. Polym. Sci., Polym. Phys. Ed.* **1974**, *12*, 941−75.
(24) Schmidt, P.; Dybal, J.; Rodriguez-Cabello, J. C.; Reboto, V. *Biomacromolecules* **2005**, *6*, 697−706.
(25) Middaugh, C. R.; Mach, H.; Ryan, J. A.; Sanyal, G.; Volkin, D. B. *Methods Mol. Biol.* **1995**, *40*, 137−56.
(26) Tiffany, M. L.; Krimm, S. *Biopolymers* **1968**, *6*, 1767−70.
(27) Stapley, B. J.; Creamer, T. P. *Protein Sci.* **1999**, *8*, 587−95.
(28) Bochicchio, B.; Ait-Ali, A.; Tamburro, A. M.; Alix, A. J. P. *Biopolymers* **2004**, *73*, 484−93.
(29) Creamer, T. P.; Campbell, M. N. *Adv. Protein Chem.* **2002**, *62*, 263−82.
(30) Lefevre, T.; Subirade, M. *Int. J. Food Sci. Technol.* **1999**, *34*, 419−28.
(31) Haris, P. I.; Chapman, D. *Methods Mol. Biol.* **1994**, *22*, 183−202.
(32) Prestrelski, S. J.; Byler, D. M.; Thompson, M. P. *Int. J. Pept. Protein Res.* **1991**, *37*, 508−12.
(33) Hollosi, M.; Majer, Z.; Ronai, A. Z.; Magyar, A.; Medzihradszky, K.; Holly, S.; Perczel, A.; Fasman, G. D. *Biopolymers* **1994**, *34*, 177−85.
(34) Mantsch, H. H.; Perczel, A.; Hollosi, M.; Fasman, G. D. *Biopolymers* **1993**, *33*, 201−7.
(35) Susi, H.; Byler, D. M. *Methods Enzymol.* **1986**, *130*, 290−311.
(36) Krimm, S.; Bandekar, J. *Adv. Protein Chem.* **1986**, *38*, 181−364.
(37) Sane, S. U.; Cramer, S. M.; Przybycien, T. M. *Anal. Biochem.* **1999**, *269*, 255−72.
(38) Eker, F.; Griebenow, K.; Cao, X.; Nafie, L. A.; Schweitzer-Stenner, R. *Proc. Natl. Acad. Sci. U.S.A.* **2004**, *101*, 10054−9.
(39) Krimm, S. Peptides and proteins. In *Raman Spectra and the Conformations of Biological Macromolecules*; Spiro, T. G., Ed.; John Wiley & Sons: New York, 1987; Vol. 1, pp 1−45.
(40) Thomas, G. J., Jr.; Prescott, B.; Urry, D. W. *Biopolymers* **1987**, *26*, 921−34.
(41) Urry, D. W.; Chang, D. K.; Krishna, N. R.; Huang, D. H.; Trapane, T. L.; Prasad, K. U. *Biopolymers* **1989**, *28*, 819−33.
(42) Girotti, A.; Reguera, J.; Arias, F. J.; Alonso, M.; Testera, A. M.; Rodriguez-Cabello, J. C. *Macromolecules* **2004**, *37*, 3396−400.
(43) Urry, D. W.; Luan, C.-H.; Peng, S. Q. *Ciba Foundation Symp.* **1995**, *192*, 4−30.
(44) Li, B.; Daggett, V. *J. Muscle Res. Cell Motil.* **2002**, *23*, 561−73.
(45) Burchard, W. *Adv. Polym. Sci.* **1999**, *143*, 113−94.
(46) Burchard, W.; Schmidt, M. *Ber. Bunsen-Ges.* **1979**, *83*, 388−91.
(47) Schmidt, M.; Nerger, D.; Burchard, W. *Polymer* **1979**, *20*, 582−8.
(48) Makhatadze, G. I.; Clore, G. M.; Gronenborn, A. M. *Nat. Struct. Biol.* **1995**, *2*, 852−5.
(49) Reiersen, H.; Clarke, A. R.; Rees, A. R. *J. Mol. Biol.* **1998**, *283*, 255−64.
(50) Karle, I. L.; Urry, D. W. *Biopolymers* **2005**, *77*, 198−204.
(51) Schmidt, P.; Dybal, J.; Rodriguez-Cabello, J. C.; Alonso, M. *Biopolymers* **2001**, *62*, 150−7.
(52) Kurkova, D.; Kriz, J.; Schmidt, P.; Dybal, J.; Rodriguez-Cabello, J. C.; Alonso, M. *Biomacromolecules* **2003**, *4*, 589−601.

MA060915J